Journal of Power Sources 391 (2018) 51–58

Contents lists available at ScienceDirect

Journal of Power Sources

journal homepage: www.elsevier.com/locate/jpowsour

Toward efficient Li-ion cells at high temperatures: Example of TiSnSb material

Lénaïc Madec[a,b,d,*], Grégory Gachot[c,d], Gaël Coquil[a], Hervé Martinez[b,d], Laure Monconduit[a,d]

[a] ICG-AIME, Bat 15, cc 15-02, Université Montpellier 2, Pl. E. Bataillon, 34095 Montpellier cedex 5, France
[b] Université de Pau et des Pays de l'Adour / CNRS UMR 5254, IPREM, 2 Av. Pierre Angot, 64053 Pau, France
[c] Laboratoire de Réactivité et Chimie des Solide (LRCS), CNRS, UMR 7314, Université de Picardie Jules Verne, 33 rue Saint Leu, Amiens, France
[d] Réseau sur le Stockage Electrochimique de l'Energie (RS2E), CNRS FR3459, 33 Rue Saint Leu, 80039 Amiens Cedex, France

HIGHLIGHTS

- Superior Li-ion cell lifetime was obtained at high temperature using TiSnSb-based electrodes.
- XPS revealed the formation of more stable and passivating SEI films at high temperature.
- GC/MS revealed a lower reactivity of the electrolyte additives at high temperature.

GRAPHICAL ABSTRACT

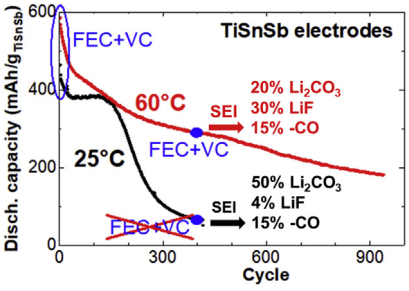

ARTICLE INFO

Keywords:
TiSnSb electrodes
High temperature
XPS
GC/MS

ABSTRACT

Developing efficient Li-ion cells with long lifetime for high temperature applications remains a challenging problem due to severe electrolyte degradation. Here, it is showed that superior lifetime, CE and polarization could be obtained at 60 °C compared to 25 °C when TiSnSb/Li coin cells filled with 1 M $LiPF_6$ EC:PC:3DMC + 5% FEC + 1% VC electrolyte were used. To understand such unexpected phenomenon, a thorough correlation of the electrochemical performance with complementary gas chromatography coupled with electron impact mass spectrometry (GC/MS) and X-ray photoelectron spectroscopy (XPS) analysis was performed. XPS results showed the formation of a more stable and passivating SEI film at the TiSnSb electrode surface at 60 °C due to a specific reactivity of the electrolyte. In good agreement, the GC/MS analysis showed only a partial consumption/reactivity of the FEC/VC additives at 60 °C while a full consumption of the additives and a further degradation of the EC solvent were observed at 25 °C. As a whole, the XPS and GC/MS results allowed to identify the origin of the superior electrochemical performance of the TiSnSb/coin cells at 60 °C.

1. Introduction

Developing efficient Li-ion cells for high temperature applications with a lifetime exceeding a decade remains one of the most challenging problems for battery researchers. The main issue remains the severe electrolyte degradation that occurs at high temperature [1] and leads to resistive electrode/electrolyte interfaces, poor performance and short lifetime [2]. To overcome such limitation, the use of electrolyte additives is one of the most simple, economical and effective approaches [3–5]. Vinylene carbonate (VC) [6–8] and fluoroethylene carbonate (FEC) [9] are known to hinder the detrimental and unwanted parasitic reactions of electrolyte solvents and/or salts occurring at the

* Corresponding author. IUniversité de Pau et des Pays de l'Adour / CNRS UMR 5254, IPREM, 2 Av. Pierre Angot, 64053 Pau, France.
E-mail address: lenaic.madec@univ-pau.fr (L. Madec).

https://doi.org/10.1016/j.jpowsour.2018.04.068
Received 1 December 2017; Received in revised form 12 February 2018; Accepted 19 April 2018
Available online 26 April 2018
0378-7753/

electrolyte/electrode interfaces during cycling and storage at high temperature through a modification of the solid electrolyte interphase (SEI) [10]. Some issues have been, however, pointed out using these additives which further emphasizes the challenge to develop efficient high temperature Li-ion cells. For instance, VC-containing cells have shown gas evolution issue at high temperature [6,11]. Similarly, both VC and FEC -containing cells showed an increase of capacity loss during storage of Li/Graphite cells between 30 and 60 °C compared to a control cells [12]. Another approach to stabilize the electrolyte reactivity at high temperature consists in replacing the commonly used and unstable $LiPF_6$ salt [13] by a more stable salt such as LiBOB [14].

Carbon-based negative electrodes that are the most used negative electrodes have also shown detrimental effect of both cycling and storage at high temperature. Andersson et al. [15] showed that precycled graphite/Li half-cells in 1 M $LiPF_6$ or 1 M $LiBF_4$ in EC:DMC (2:1 in volume) had increasing amount of LiF deposited at their surface while the storage temperature increased up to 80 °C which indicates a large degradation of the Li salts. Araki et al. [16] similarly observed the decomposition of the $LiPF_6$ salt when $LiMn_{1.7}Al_{0.3}O_4$/hard carbon cells were stored in 1 M $LiPF_6$ in EC:DEC:DMC (1:1:1 in volume) at 65 °C with an increasing amount of PO_4^{3-} component found in the SEI film analysed by XPS. Bodenes et al. [17] also showed that cycling Li (Ni,Mn,Co) O_2/graphite cells in carbonate solvents using 1 M $LiPF_6$ at 85 °C led to a decrease of carbonate species at the graphite surface simultaneously with an increase of inorganic compounds arising from salt degradation, as observed using XPS.

In the case of transition metal oxide and post-transitional elements -based negative electrodes, however, only few studies report the high temperature performance despite that surprising behavior have been observed. Grugeon et al. [18] showed that Co nanoparticles-based electrodes such as CoO underwent capacity increase during cycling in 1 M $LiPF_6$ EC:DMC (1:1 in weight) at high temperature, especially at 75 °C. A similar phenomenon, was also observed in the case of Cu_3N-based electrodes cycled in 1 M $LiPF_6$ EC:DMC (1:1 in weight) at 70 °C compared to room temperature [19] as well as for chromium oxides-based electrodes cycled in 1 M LiTFSI EC at 100 °C compared to 50 °C [20]. These results suggest that the metal oxides or the 3d-metal nature does not govern such capacity increase. The role of the high temperature on such anomalous capacity increase remains, however, unclear as similar phenomena were also observed at room temperature using α-Fe_2O_3-based electrodes cycled in 1 M $LiPF_6$ in EC:DMC (1:1 in volume) [21,22] or CoO-based electrode in 1 M $LiPF_6$ EC:DMC (1:1 in weight) [23]. In this latter case, the conversion reaction of CoO with Li at 0.8 V vs. Li/Li^+ was followed by an additional capacity down to 0.01 V. This was explained to the formation of a polymer-like film around the catalytic nanoparticles from the electrolyte degradation for which a reversible dissolution/reformation was observed during charge/discharge using TEM. Moreover, such polymer-like film was found beneficial to the cycle life when varying the cycling potential window probably because it maintains the cohesion between the nanoparticles [24]. The polymer-like film was identified as phosphate-ending ethylene oxide oligomers (CH_2-CH_2-O) chains using FTIR [25], mass spectrometry [26,27], and XPS [28]. However, the origin of the extra capacity associated with the polymer-like film still remains unclear [29] although additional interfacial Li storage mechanism have been proposed in the studies of RuO_2 [30] and NiO [31] -based electrodes.

Recently, TiSnSb was reported as a promising conversion material for negative electrodes at room temperature [32] with improved performance using CMC as binder [33] and FEC and VC as electrolyte additives [34]. Here, the effects of high temperature on the reactivity and electrochemical performance of TiSnSb-based electrodes was investigating. Electrochemical performance of TiSnSb/Li coin cells at both 25 °C and 60 °C were correlated to X-ray photoelectron spectroscopy (XPS) of the SEI films formed during formation and after long term cycling. Gas chromatography coupled with electron impact mass spectrometry (GC/MS) analysis was also performed to identify the reactivity of the electrolyte components (solvents and additives).

2. Experimental

2.1. Material synthesis and electrodes preparation

TiSnSb was prepared by mechanical grinding, from 1 g of Ti (~100 mesh, 99.5% purity, Alfa-Aesar), Sn (purity ≥99%, Aldrich) and Sb (~325 mesh, 99.5% purity, Alfa-Aesar) powders with a 1.1:1:1 molar ratio, for 8 h under Ar atmosphere using a SPEX 8000 M Mixer/Mill. The TiSnSb diffractogram was recorded using an X'pert diffractometer equipped with Cu Kα radiation in the range $10 < 2\theta < 70°$ and the profile matching of the TiSnSb diffractogram [35] was confirm using the FULLPROF software (Fig. S1). Electrodes were then prepared by mixing TiSnSb, acetylene black (Y50A, BET = 70 m^2/g, SN2A), vapor ground carbon fibers (VGCF-S, BET = 15 m^2/g, Showa Denko) and carboxymethyl cellulose (CMC, DS = 0.7, Mw = 250 000, Aldrich) with a 70:9:9:12 weight ratio in deionized water (0.8 ml) using a silicon nitride vial and a planetary ball-milling for 1 h. The obtained slurry was then tape casted on a 17.5 µm thick copper foil (99.9%, Goodfellow) with a 150 µm thickness and dried for 24 h at room temperature. Electrodes with a 12.7 mm diameter were then punched out and dried for another 15 h at 120 °C under vacuum. The final active material loading of the electrode was 3 mg cm^{-2} ± 0.3 mg.

2.2. Cells preparation and cycling protocol

The electrolyte used in this study was 1 M $LiPF_6$ (battery grade, purity ≥99.99%, Aldrich) in EC (anhydrous, 99% purity, Aldrich):PC (anhydrous, 99.7% purity, Aldrich):DMC (anhydrous, purity ≥99%, Aldrich) with a 1:1:3 vol ratio to which 5% FEC (98% purity, Alfa Aesar) and 1% VC (80 ppm BHT as stabilizer, 99% purity) were added. The water content measured by Karl-Fischer titration was lower than 50 ppm. 2032 coin cells were assembled in an argon-filled glove box by stacking a lithium foil as counter and reference electrode, a glass-fiber paper (GF/D, Whatman) and a polypropylene-polyethylene-polypropylene (PPP) membrane separator (Celgard) as separator and a TiSnSb electrode soaked in 0.20 ml of electrolyte.

All tests were carried out using a Neware Battery Testing System under galvanostatic mode from 0.02 to 1.5 V vs. Li^+/Li. For each electrochemical experiments, at least two identical coin cells were prepared for reproducibility. Cells were placed either in a temperature-controlled room at 25 ± 1 °C or in an oven set at 60. ± 0.1 °C then discharge to 0.02 V at C/2 rate (*i.e.* 0.5 mole of Li per mole of TiSnSb per hour), followed by a 48 h storage period and charge to 1.5 V at C/2. After this formation cycle, cells were cycled between 0.02 and 1.5 V at 4C (*i.e.* 4 mole of Li per mole of TiSnSb per hour) at 25 °C or 60 °C.

For XPS and GC/MS analysis, TiSnSb/Li cells were stopped after 400 ± 25 cycles for both 25 °C and 60 °C to allow a direct comparison while for the electrochemical long term cycling at 60 °C, additional cells were cycled up to ~900 cycles. For XPS and GC/MS analysis, coin cells were carefully disassembled in an argon-filled glove box. The glass-fiber paper and PPP membrane separators were store in polypropylene tubes (Eppendorf) before to be used for GC/MS analysis. TiSnSb electrodes were washed twice by immersion into 1 mL of DMC (anhydrous, ≥99% purity, Aldrich) in a clean and dry glass vial with a mild manual agitation for 10 s to remove the majority of the $LiPF_6$ salt. Air sensitive samples were then kept sealed under Argon in polypropylene tubes (Eppendorf) before to be analysed by XPS.

2.3. Gas chromatography coupled with electron impact mass spectrometry (GC/MS)

All analyses were performed using a trace 1300 serie GC ultra gas chromatograph (Thermo Scientific). The chromatographic separation was performed on a “BPX70” cyanopropyl polysilene-siloxane based

capillary column (30 m × 0.25 mm i.d., 0.25 µm) from SGE. Helium was used as the GC carrier gas and maintained at a constant flow rate of 1.3 mL/min. To achieve good chromatographic peaks resolution, the programmable temperature gradient was optimized from 40° to 250 °C as follows: the capillary column was ramped from the initial temperature of 40 °C, held for 5 min, increased at 10 °C/min up to 250 °C where it was held for 10 min. The total duration of GC analysis was 36 min. The transfer line was maintained at 250 °C. The ion source was set at 200 °C.

The GC was interfaced with an ISQ mass spectrometer (Thermo Scientific).

Tuning of the mass spectrometer was done automatically using the ions resulting from perfluorotributylamine ionization. The mass spectrometer was operated with a filament current of 250 µA and electron energy of 70 eV in the electron ionization (EI) mode. The mass range was 10–300 u and data acquisition and processing were performed with Xcalibur 2.0.7 software. Compounds identification and corresponding structural formulae were assigned using the National Institutes of Standards (NIST) library.

2.4. X-ray photoelectron spectroscopy (XPS)

XPS was performed with a Kratos Axis Ultra spectrometer using a focused monochromatized Al Kα radiation (hν = 1486.6 eV). The XPS spectrometer was directly connected through an argon-filled glove box in order to avoid moisture/air exposure of the samples. All samples were kept at 10^{-8} mbar for one night before analysis to ensure a strictly identical vacuum procedure. The analysed sample area was 300 µm × 700 µm. Core spectra were recorded with a constant pass energy of 20 eV at an operating pressure $< 2 \times 10^{-8}$ mbar. Short-time spectra were recorded at the beginning to follow any possible sample degradation under the X-ray beam. Note that form long term cycling samples, the sample stage was cooled down to −150 °C to prevent degradation that was observed when analysis was performed at room temperature. Short-time spectra were also recorded for two different area for each samples to ensure that samples surface was homogeneous so that the results presented here are representative of the whole electrode. Data treatment was performed using CasaXPS software and the binding energy scale was calibrated from the C1s peak at 285 eV (C-C/C-H). A non-linear Shirley-type background [36] was used for core peaks analysis while 70% Gaussian - 30% Lorentzian Voigt peak shapes and full width at half-maximum (fwhm) constraint ranges were selected to optimize areas and peak positions.

3. Results and discussion

3.1. Electrochemical performance

Fig. 1a shows the cell potential versus capacity (mAh/$g_{active\text{-}material}$) during the first (C/2) and second (4C) cycles for the TiSnSb coin cells cycled between 0.02 and 1.5 V at 25 °C and 60 °C. Fig. 1b shows a summary of the coulombic inefficiency (1 - coulombic efficiency (CE), referred to as CIE) for the same cells. At both 25 °C and 60 °C, similar galvanostatic discharge/charge profiles were observed with a rapid decrease of the potential down to 0.8 V followed by the conversion reaction of TiSnSb into $Li_3Sb/Li_7Sn_2/Ti$ as described previously [32,37]. At 60 °C, an additional electrochemical phenomenon was observed during the first cycle at ~1.35 V as indicated by an arrow in Fig. 1. While this could be explained either by a specific reactivity of the electrolyte or by the reaction of the TiSnSb surface oxide layer with lithium, the exact nature remains unclear. Moreover, the discharge capacity of the first cycle was higher than the theoretical one (580 mA h/g_{AM}) for both 25 °C (615 mA h/g_{AM}) and 60 °C (680 mA h/g_{AM}) due to the reduction of electrolyte components in addition to the Li_3Sb and Li_7Sn_2 formation. This phenomenon was more pronounced at 60 °C and is associated to a higher coulombic inefficiency (1 - CE, CIE)

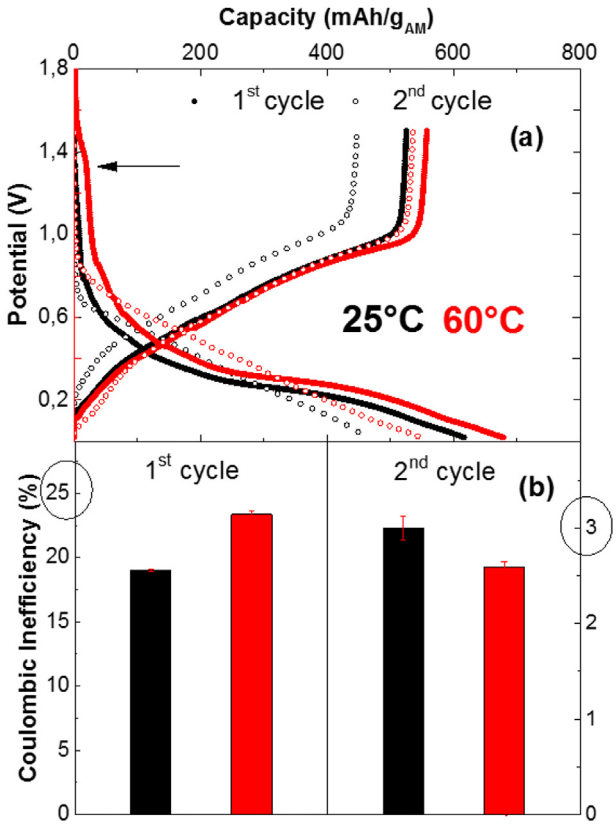

Fig. 1. (a) Cell potential versus capacity during the first (C/2) and second (4C) cycles of the TiSnSb/Li coin cells filled with 1 M $LiPF_6$ EC:PC:3DMC + 5% FEC + 1% VC and cycled between 0.02 and 1.5 V at 25 °C and 60 °C; (b) Coulombic inefficiency (CIE) associated with the first and second cycles for the same cells. In panel (a), the galvanostatic curve for only one cell is presented for each temperature for better clarity while in panel (b), the CIE are the average data of two pair cells and the standard deviation of the data is represented by the error bars.

for the first cycle compared to 25 °C (Fig. 1b) as expected by the temperature dependence of the parasitic reactions. During the second cycle, both 25 °C and 60 °C showed a greatly decreased CIE with, however, a higher CIE at 25 °C compared to 60 °C. While this may be due to enhanced reversible conversion processes at 60 °C, lower parasitic reactions may also occur. In this latter case, it suggests that a relatively more stable and efficient SEI film would be formed at 60 °C during the first cycle and hinder parasitic reactions during subsequent cycles.

Fig. 2a shows the discharge capacity and coulombic efficiency (CE) of the long term cycling between 0.02 and 1.5 V at 4C and 25 °C or 60 °C for the TiSnSb/Li coin cells filled with 1 M $LiPF_6$ EC:PC:3DMC + 5% FEC + 1% VC. At 25 °C, the discharge capacity was stable over the first ~200 cycles then quickly fell to become lower than 100 mA h/g_{AM} after ~300 cycles. At 60 °C, although the discharge capacity continuously decreased over the entire cycling, a higher capacity retention was observed with ~200 mA h/g_{AM} after ~900 cycles. This result is therefore unexpected considering the large extent of parasitic reactions [1] and the concomitant poor performance and shorter lifetime [2,6] normally observed when Li-ion cells are exposed to high temperature. Moreover, the evolution of CE showed an odd behavior at both temperatures with a sudden decrease after ~100 cycles until a reverse point where the CE continuously increased until the end of the cycling. The sudden decrease of CE may be due to a breaking of the SEI film and/or the electrode cohesion, which would increase the parasitic reactions. This phenomenon would then worsen until the formation of a highly passivating SEI film. At this point, both the TiSnSb lithiation/delithiation processes and the parasitic reactions would become

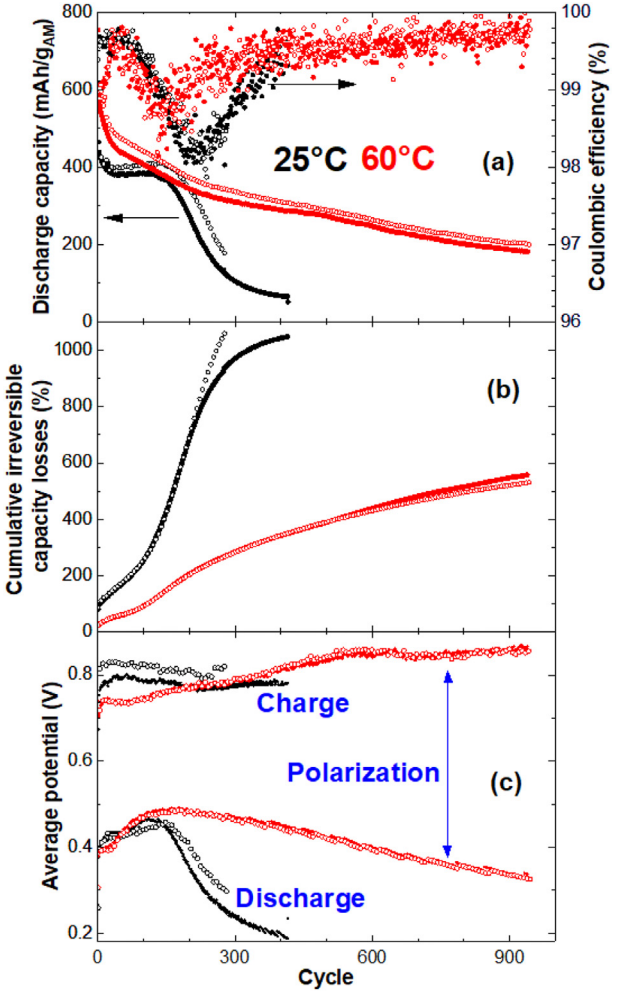

Fig. 2. (a) Discharge capacity and coulombic efficiency (CE) as function of cycle number of TiSnSb/Li coin cells filled with 1 M $LiPF_6$ EC:PC:3DMC + 5% FEC + 1% VC and cycled between 0.02 and 1.5 V at 4C for 25 °C or 60 °C; (b) Cumulative irreversible capacity losses (%) and (c) average discharge/charge potentials (V) as function of cycle number for the same cells.

hindered which should lead to an increase of the CE as observed. At 60 °C, however, this overall phenomenon was less pronounced and no sudden capacity decrease was observed may be due to an enhanced TiSnSb lithiation/delithiation kinetics. In any case, the CE became quickly higher at 60 °C compared to 25 °C, which explains the much lower and slower cumulative irreversible capacity losses observed at 60 °C (Fig. 2b). The average potential in discharge/charge also points out the superior performance of the 60 °C cycling with a more stable and lower polarization compared to 25 °C (Fig. 2c). This result can be explained by an enhanced TiSnSb lithiation/delithiation kinetics at 60 °C. Note that for both temperature, the average potential in charge was quite stable while in discharge it first increased then decreased after ~150 cycles with a much more pronounced effect at 25 °C. While this result may correlate to the evolution of the CE, the exact reason remains unclear. It only suggests that the TiSnSb lithiation processes becomes hindered by a thickening of the SEI films while the delithiation processes would be less impacted.

3.2. Consumption of the electrolyte components

Fig. 3 shows the chromatograms of (a) the 1 M $LiPF_6$ EC:PC:3DMC + 5% FEC + 1% VC electrolyte after storage in a glass vial for 3 weeks as well as the electrolyte extracted from the TiSnSb/Li coin cells filled with 1 M $LiPF_6$ EC:PC:3DMC + 5% FEC + 1% VC (b) after storage for 3 weeks, (c) after the first discharge (C/2) at 0.02 V and (d) after the long term cycling at 1.5 V on charge for both 25 °C and 60 °C. It is reminded that for both XPS and GC/MS analysis, TiSnSb/Li cells were stopped after 400 ± 25 cycles for both 25 °C and 60 °C to allow a direct comparison.

After storage in a glass vial for 3 weeks (Fig. 3a), the electrolyte color was yellow and black at 25 °C and 60 °C, respectively (not shown). In both cases, very close ratio of carbonate solvents and additives were observed. Two additional peaks with a relatively low abundance were, however, observed at 60 °C. These peaks are attributed to the formation of carbonate degradation compounds due to the reaction of the carbonate solvents with the thermal degradation products of the $LiPF_6$ salt at high temperature [38]. This result is in good agreement with the appearance of two F- and P-based compounds at 60 °C, that can only originate from the $LiPF_6$ salt, as observed by ^{19}F and ^{31}P NMR (Fig. S2). Note also that no additional peak was observed by GC/MS when the $LiPF_6$ salt was replace by LiTFSI (Fig. S2). Surprisingly, the electrolyte extracted from the TiSnSb/Li coin cells after storage at 60 °C for 3 weeks (Fig. 3b) showed no additional peak, which suggests that the previous reactivity was suppressed when the electrolyte was in contact with the electrodes. This is supported by the absence of any color of the separator soaked by the electrolyte while the electrolyte stored at 60 °C in a glass vial was dark after 3 weeks. At this point, it is suggested that the TiSnSb electrode may somehow scavenge the $LiPF_6$ decomposition products although the exact mechanism remains unclear so far. The electrolyte extracted from the TiSnSb/Li cells after storage showed, however, a similar decrease of the EC/PC ratio whatever the temperature was more likely due to a consumption/degradation of the EC solvent. Considering that carbonate solvents are well known to be highly reactive against metallic Li, a preferential reactivity of the EC with the metallic Li electrode in such TiSnSb/Li coin cells can not be excluded although the exact nature of this phenomenon remains unclear.

After the first discharge (Fig. 3c), no detectable change was observed, whatever the temperature was, compared to the electrolyte stored in glass vial at 25 °C (Fig. 3a). Note that no further change was observed after the first cycle (not shown). These results suggest that neither the first electrochemical cycle nor the temperature (for the corresponding time) has any detectable impact on the consumption/degradation of the solvents and additives. After long term cycling (Fig. 3d), however, significant changes were observed. At 25 °C, the additives were not detected anymore and the EC/PC ratio drastically decreased. Surprisingly, at 60 °C, low amount of additives were, however, still detected and the EC/PC was retained. These results mean that at 25 °C, both VC and FEC were fully consumed then EC was consumed. At 60 °C, VC and FEC were partially consumed and the solvents did not appear reactive. Therefore, cycling at 25 °C more likely lead to the formation of a poorly stable SEI film so that additives are continuously consumed during long term cycling followed by the further degradation of the solvents. At 60 °C, however, a more stable SEI film should be formed which hinders the full consumption of the additives as well as the solvents degradation. This is therefore unexpected considering the severe electrolyte degradation usually reported at high temperature [1,2,6]. In any case, these GC/MS results are in good agreement with the superior capacity retention and higher CE of the TiSnSb/Li cells observed for the long term cycling at 60 °C compared to 25 °C (Fig. 2).

3.3. Electrodes surface analysis

Fig. 4 shows (a) the Carbon 1s, (b) the Oxygen 1s and Antimony 3d as well as (c) the Tin 3d XPS core spectra of the fresh TiSnSb electrode and TiSnSb electrodes as taken from the TiSnSb/Li coin cells filled with 1 M $LiPF_6$ EC:PC:3DMC + 5% FEC + 1% VC electrolyte after storage for 3 weeks, after the first discharge (C/2) at 0.02 V and after the long term cycling (~400 cycles at 4C) at 1.5 V on charge for both 25 °C and 60 °C. Table 1 shows the XPS quantification data (in at.%) for the same

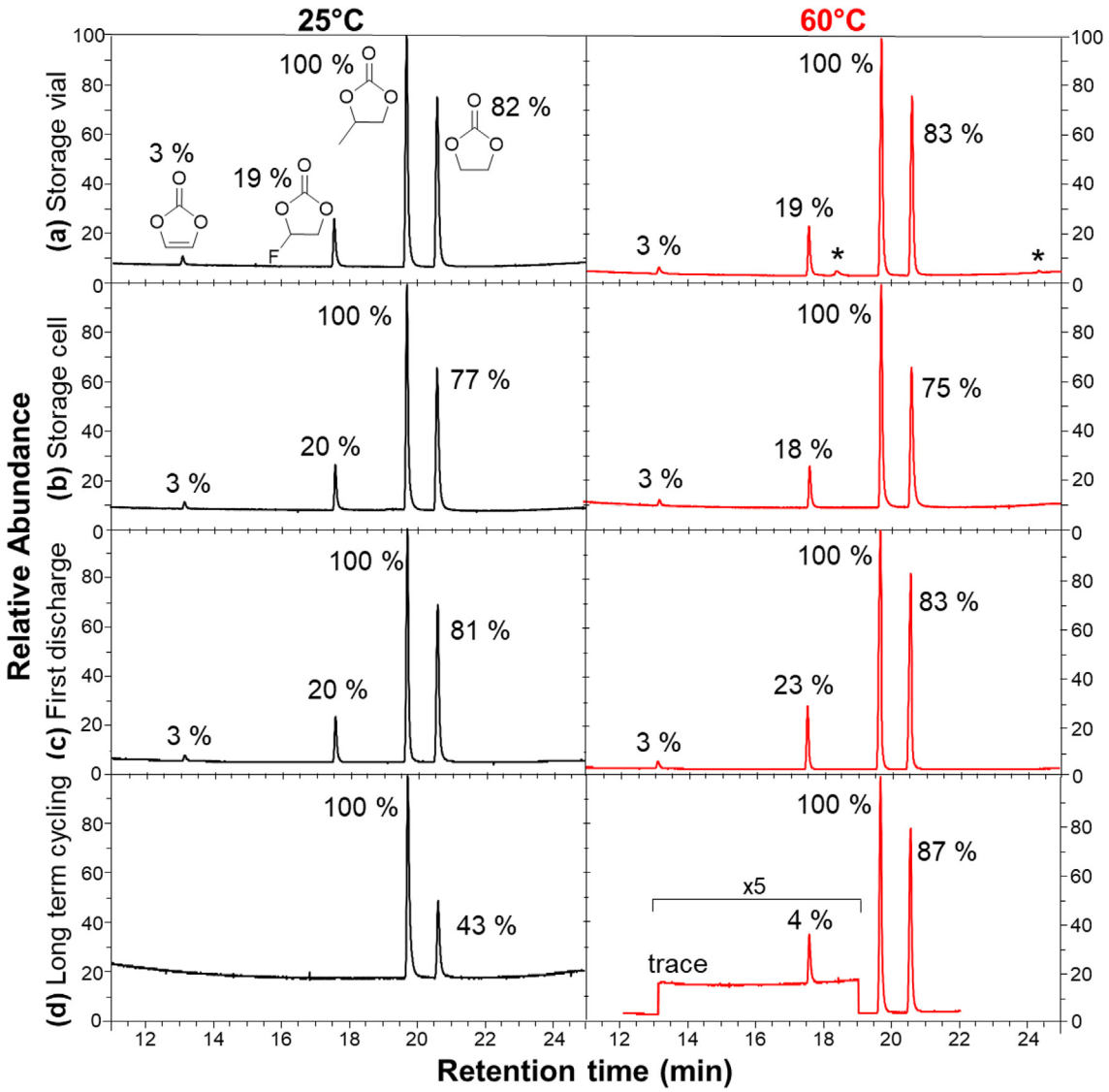

Fig. 3. Chromatograms of the 1 M $LiPF_6$ EC:PC:3DMC +5% FEC +1% VC electrolyte (a) after storage in glass vials for 3 weeks, (b) after storage of TiSnSb/Li coin cells for 3 weeks, (c) after the first discharge (C/2) of TiSnSb/Li coin cells to 0.02 V and (d) after long term cycling of TiSnSb/Li coin cells (~400 cycles at 4C) at 1.5 V on charge for both 25 °C and 60 °C. For all chromatograms, the relative abundance of the peak attributed to PC was always the highest and therefore normalized to 100%. Values in percentages give the integrated intensity of each peak compared to the integrated intensity of PC, so the percentage indicated here are used to follow the evolution of the different electrolyte components. Note that according to our experimental setup, the retention time of DMC is very close to the one of the CH_3CN use for extraction (6 min) so the DMC peak is never shown.

electrodes. In Fig. 4, core level spectra of the fresh TiSnSb electrode were maximized to show low intensity peaks while for stored/cycled TiSnSb electrodes, core level spectra for a given element were normalized to allow a direct comparison of the relative intensities/amount of the given element between samples.

Fresh TiSnSb electrode - The C 1s core spectrum (Fig. 4a) showed seven components at 284.5, 285.0, 286.1, 287.4, 289.0, 290.3 and 291.2 eV assigned to the C=C, C-C/C-H and -CO from the carbon additives, -CO and $-CO_2$ from the CMC binder, $-CO_3$ and ''shake up'' satellite from the carbon additives, respectively [39–41]. The O 1s core spectrum (Fig. 4b) showed three peaks at 530.8, 532.1 and 533.8 eV attributed to Sn/Sb oxide layer at the TiSnSb surface [37] as well as -CO and $-CO_2$/$-CO_3$ from the CMC binder and carbon additives, respectively [41,42]. The Sb 3d core spectrum showed two doublets at 527.9–537.3 and 531.2–540.6 eV attributed to metallic Sb and the Sb oxide layer from the TiSnSb material. An additional peak was also observed at 536.7 eV due to Na Auger from the CMC binder [43]. The Sn 3d core spectrum (Fig. 4c) showed two doublets at 484.5–492.9 and 486.7–495.1 eV assigned to metallic Sn and a Sn oxide layer from the TiSnSb material. Two Na Auger components were also observed at 497.5 and 501.8 eV.

TiSnSb electrodes after storage - At 25 °C, the contribution of the carbon additives components decreased while at 60 °C it remained close to the fresh electrode (Fig. 4a and Table 1). This indicates the formation of a SEI film at the carbon additives surface when stored at 25 °C while almost no covering seems to occur at 60 °C. Note that the appearance of a second carbon additives component at 282–283 eV, more important at 60 °C, more likely originates from a differential charging effect [44]. In the O 1s spectra (Fig. 4b), the two main peaks of the fresh electrode were replaced by two new components at 531.7 and 533.1 eV due the simultaneous covering of the CMC binder and the carbon additives by a SEI film [41]. Considering the lower amount of Na (Table 1) and the lower Na Auger components on the Sn 3d core spectra (Fig. 4c) at 60 °C, the CMC binder appears more covered at 60 °C. The Sn core spectra after storage (Fig. 4c) showed a significant decrease of the Sn oxide peak due to the formation of a SEI film at the TiSnSb surface. This is

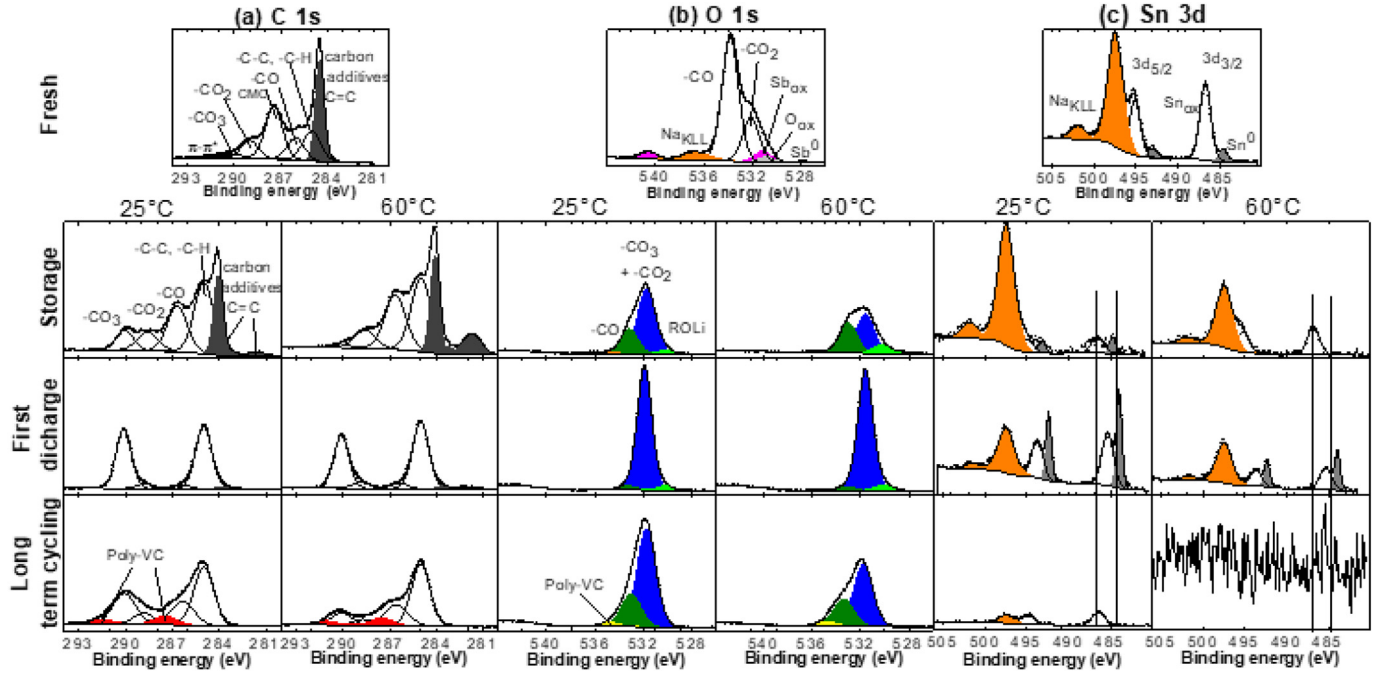

Fig. 4. (a) Carbon 1s, (b) Oxygen 1s and Antimony 3d as well as (c) Tin 3d XPS core spectra of the fresh TiSnSb electrode and TiSnSb electrodes as taken from the TiSnSb/Li coin cells filled with 1 M $LiPF_6$ EC:PC:3DMC + 5% FEC + 1% VC electrolyte after storage for 3 weeks, after the first discharge (C/2) at 0.02 V and after the long term cycling (~400 cycles at 4C) at 1.5 V on charge for both 25 °C and 60 °C.

supported by the absence of Sb peak (Fig. 4b). However, a larger amount of Sn oxide was observed at 60 °C (Table 1) while the Sn metal peak was observed only at 25 °C suggesting a specific reactivity of the Sn/Sb elements. As a whole, a different coverage/reactivity of the carbon additives, the CMC and the Sn of the TiSnSb material was observed after storage for 3 weeks between 25 °C and 60 °C so that the SEI films inhomogeneously cover the different components of the TiSnSb electrodes.

Regarding the SEI composition after storage, the peak at 531.7 eV on the O 1s core spectra (Fig. 4b) is attributed to Li_2CO_3 and other $ROCO_2Li$ carbonate compounds [45,46] while the peak at 533.1 eV is assigned to -CO bonds from ether derivatives and/or $ROCO_2Li$ [47,48]. At 25 °C, the SEI is therefore dominated by Li_2CO_3 while at 60 °C the SEI is dominated by ether derivatives and/or $ROCO_2Li$ as well as LiF in agreement with the C 1s core spectra (Fig. 4a and Table 1). For both temperatures, the formation of the carbonate degradation compounds

Table 1
XPS quantification data (in at.%) of the fresh TiSnSb electrode and TiSnSb electrodes as taken from the TiSnSb/Li coin cells filled with 1 M $LiPF_6$ EC:PC:3DMC + 5% FEC + 1% VC electrolyte after storage for 3 weeks, after the first discharge (C/2) at 0.02 V and after the long term cycling (~400 cycles at 4C) at 1.5 V on charge for both 25 °C and 60 °C.

		B.E. (eV)	Fresh	B.E. (eV)	Storage 25 °C	Storage 60 °C	B.E. (eV)	0.02 V 25 °C	0.02 V 60 °C	Long term cycling 25 °C	Long term cycling 60 °C
			At.%		At.%	At.%		At.%	At.%	At.%	At.%
Sn 3d	Sn metal	484.5–492.9	*0.06*	484.7–493.1	*0.04*	-	484.0–492.4	*0.12*	*0.05*	-	-
	Sn oxide	486.7–495.1	*0.4*	486.7–495.1	*0.06*	*0.1*	485.3–493.7	*0.18*	*0.08*	*0.05*	-
Sb 3d	Sb metal	527.9–537.3	*0.04*	-			–				
	Sb oxide	531.2–540.6	*0.2*	-			–				
C 1s	C=C	284.5	*17.9*	< 284.6	*10.9*	*17.3*	< 284.6	*0.8*	*1.8*	-	-
	-C-C, -C-H	285.0	*11.5*	285.0	*18.8*	*18.9*	285.0	*16.9*	*17.9*	*15.3*	*17.1*
	-CO	286.1	*8.2*	286.7	*12.7*	*15.2*	286.5	*1.3*	*1.7*	*7.1*	*7.6*
	-CO (CMC)	287.4	*19.4*	–			–				
	$-CO_2$ (CMC)	289.0	*6.4*	–			–				
	$-CO_2$	–		288.6	*5.6*	*5.2*	288.8	*1.4*	*1.9*	*3.1*	*1.8*
	$-CO_3$	290.3	*1.6*	290.1	*4.7*	*0.9*	290.0	*14.8*	*12.9*	*8.8*	*3.6*
	π-π*	291.2	*1.0*	–			–				
	Poly-VC	–		–			287.5–291.5	-	-	*3.8*	*3.7*
O 1s	ROLi	–		530			530	*1.5*	*2.1*	-	-
	Sb, Sn oxide	530.8	*0.6*	–	*1.1*	*2.4*	–				
	$-CO_3$, $-CO_2$	532.1	*5.2*	531.7	*18.4*	*11.0*	531.7	*35.5*	*34.2*	*28.0*	*17.5*
	-CO	533.8	*14.4*	533.1	*6.7*	*8.1*	533.2	*1.3*	*1.27*	*9.9*	*8.2*
	Poly-VC	–					534.7	-	-	*1.15*	*1.1*
F 1s	LiF	–		685.2	*1.6*	*4.6*	684.8	-	-	*2.3*	*14.6*
	Others	–		687.4	*0.2*	*0.5*	> 687	-	-	*1.3*	*4.8*
Li 1s	Total	–		55.4	*10.3*	*9.9*	55.4	*26.2*	*26.1*	*19.2*	*18.9*
P 2p	Total	–		133.4	-	*1.2*	133.8–137.7	-	-	-	*1.1*
Na 1s	Na (CMC)	1071.6	*13.1*	1071.6	*8.9*	*4.7*	–				

are believed to mainly originate from the reactivity of the EC solvent as suggested by the decrease of the EC/PC ratio (Fig. 3).

TiSnSb electrodes after the first discharge - For both temperature, the carbon additives peaks significantly decreased (Fig. 4a). This phenomenon was, however, slightly more pronounced at 25 °C indicating the formation of a thicker SEI film at the carbon additives surface during the first discharge compared to 60 °C, as similarly observed after storage. It is therefore an unusual behavior compared to conventional graphite-based negative electrodes [1,2,6]. In the case of the Sn components (Fig. 4c), an intensity decrease was also observed after the first discharge for both temperature. This phenomenon was, however, more important at 60 °C indicating the formation of a thicker SEI film at the TiSnSb surface. Contrary to the Sn, no Sb peak was observed after the first discharge whatever the temperature was as similarly observed after storage (Fig. 4b). These results again highlight a specific reactivity of the Sn/Sb elements of the TiSnSb material towards the electrolyte. Considering that Li_3Sb and Li_7Sn_2 phases are formed during the first discharge [32], it may indicate that the Li_3Sb and Li_7Sn_2 particles would be fully and partially covered by the SEI, respectively. Additionally, for both temperature, similar Na Auger components (Fig. 4c) were observed due to a similar covering of the CMC binder by the SEI film.

Regarding the SEI composition after the first discharge, no significant difference was observed between 25 °C and 60 °C. Both SEI films were mainly formed of Li_2CO_3 as observed on the C 1s and O 1s core spectra while no F- or P-based species were detected (Table 1) in good agreement with the GC/MS data for which no detectable difference of electrode reactivity was observed (Fig. 3).

TiSnSb electrodes after long term cycling - For both temperature, no carbon additive peak was observed which means that relatively thick SEI films were formed at the carbon additives surfaces during long term cycling (Fig. 4a). The Na Auger components was still observed after the long term cycling but only at 25 °C which suggests a thinner and/or less homogeneous covering of the CMC binder by the SEI film compared to 60 °C (Fig. 4c). Similarly, the Sn oxide peak was only observed at 25 °C which also suggests that a thinner and/or less homogeneous SEI covering of the Sn-containing phase compared to 60 °C (Fig. 4c). These results are therefore unexpected considering that the TiSnSb conversion reactions were nearly inactive after ~400 cycles (Fig. 2) and that FEC and VC were fully consumed (Fig. 3) so that thicker SEI films were expected at 25 °C. It therefore appears that the best TiSnSb electrodes in term of electrochemical performance (*i.e.* at 60 °C) formed thicker and/or more homogeneous SEI films. In any case, the SEI films formed at 60 °C should be more stable and/or more accommodating against the successive lithiation/delithiation processes of the TiSnSb conversion material. The higher stability of the SEI at 60 °C is well supported by the partial consumption of FEC and VC and the higher stability of the EC/PC solvents observed by GC/MS (Fig. 3). As a whole, whereas at 60 °C a kinetic effect may favored the Li^+ ion conduction though the thick SEI films, it cannot explained, however, the higher capacity retention and CE compared to 25 °C. In any case, these results remain unexpected considering the severe electrolyte degradation [1] and resulting resistive/inactive interfaces usually reported at high temperature [2,6].

Regarding the SEI composition after long term cycling, large changes were observed compared to the first discharge. For both temperature, the amount of Li_2CO_3 decreased after cycling with, however, a more pronounced phenomenon at 60 °C (Fig. 4 and Table 1). The amount of LiF also increased but more significantly at 60 °C (Table 1). Note that other F- and P-based species were also observed with a larger content at 60 °C (Table 1) which points out a higher degradation of the $LiPF_6$ salt at 60 °C. Additionally, two new components appeared on the C 1s core spectra at 287.5 and 291.5 eV with a 2:1 ratio while one new peak was observed at 534.7 eV on the O 1s core spectra. These peaks can be explained by the formation of a polymer of VC (poly-VC) at the TiSnSb electrode surface during cycling [42,49].

4. Conclusion

In the present study, it was showed that superior electrochemical performance (lifetime, CE and polarization) could be obtained at 60 °C compared to 25 °C using TiSnSb/Li coin cells filled with 1 M $LiPF_6$ EC:PC:3DMC + 5% FEC + 1% VC electrolyte. To understand such unexpected high temperature effect, electrochemical performance were correlated with complementary GC/MS and XPS results. GC/MS allowed to analyse the consumption/reactivity of the electrolyte components. It was showed that only a partial consumption/reactivity of the FEC/VC additives occurred at 60 °C while a full consumption of the additives and a further degradation of the EC solvent occurred at 25 °C. These results suggested the formation of a poorly stable/passivating SEI film at the TiSnSb electrode surface at 25 °C compared to 60 °C. XPS analysis showed that after storage or after the first discharge, the SEI covers inhomogeneously the different components of the TiSnSb electrodes with a specific reactivity of the Sn/Sb elements towards the electrolyte. After the first discharge, however, close SEI films composition was observed at both temperature in good agreement with the GC/MS results. After long term cycling, a thicker and/or more homogeneous as well as more stable and/or passivating SEI was observed at 60 °C. As a whole, the XPS and GC/MS results allowed to identify the origin of the superior electrochemical performance of the TiSnSb/coin cells at 60 °C. Further studies are now required to extend these superior performance at high temperature to other negative electrodes as well as to positive electrodes then to full Li-ion cells.

Acknowledgements

This work was financially supported by the SATT AXLR and the Program *Investissements d'Avenir* STORE-EX No. ANR-10-LABX-76-01. L.M. also acknowledges the RS2E network for the postdoctoral grant.

Appendix A. Supplementary data

Supplementary data related to this article can be found at http://dx.doi.org/10.1016/j.jpowsour.2018.04.068.

References

[1] N.N. Sinha, T.H. Marks, H.M. Dahn, a.J. Smith, J.C. Burns, D.J. Coyle, J.J. Dahn, J.R. Dahn, The rate of active lithium loss from a soft carbon negative electrode as a function of temperature, time and electrode potential, J. Electrochem. Soc. 159 (2012) A1672–A1681, http://dx.doi.org/10.1149/2.048210jes.

[2] P. Ramadass, B. Haran, R. White, B.N. Popov, Capacity fade of Sony 18650 cells cycled at elevated temperatures: Part II. Capacity fade analysis, J. Power Sources 112 (2002) 614–620, http://dx.doi.org/10.1016/S0378-7753(02)00473-1.

[3] S.S. Zhang, A review on electrolyte additives for lithium-ion batteries, J. Power Sources 162 (2006) 1379–1394, http://dx.doi.org/10.1016/j.jpowsour.2006.07.074.

[4] K. Xu, Nonaqueous liquid electrolytes for lithium-based rechargeable batteries nonaqueous liquid electrolytes for lithium-based rechargeable batteries, Chem. Rev. 104 (2004) 4303–4418, http://dx.doi.org/10.1021/cr030203g.

[5] K. Xu, Electrolytes and interphases in batteries: advances during 2003 ~ 2014, Chem. Rev. 114 (2014) 11503–11618.

[6] J. Xia, L. Ma, J.R. Dahn, Improving the long-term cycling performance of lithium-ion batteries at elevated temperature with electrolyte additives, J. Power Sources 287 (2015) 377–385, http://dx.doi.org/10.1016/j.jpowsour.2015.04.070.

[7] W.J. Lee, K. Prasanna, Y.N. Jo, K.J. Kim, H.S. Kim, C.W. Lee, Depth profile studies on nickel rich cathode material surfaces after cycling with an electrolyte containing vinylene carbonate at elevated temperature, Phys. Chem. Chem. Phys. 16 (2014) 17062–17071, http://dx.doi.org/10.1039/c4cp02075h.

[8] W. Li, a. Xiao, B.L. Lucht, M.C. Smart, B.V. Ratnakumar, Surface analysis of electrodes from cells containing electrolytes with stabilizing additives exposed to high temperature, J. Electrochem. Soc. 155 (2008), http://dx.doi.org/10.1149/1.2949507 A648.

[9] M.H. Ryou, G.B. Han, Y.M. Lee, J.N. Lee, D.J. Lee, Y.O. Yoon, J.K. Park, Effect of fluoroethylene carbonate on high temperature capacity retention of $LiMn_2O_4$/graphite Li-ion cells, Electrochim. Acta 55 (2010) 2073–2077, http://dx.doi.org/10.1016/j.electacta.2009.11.036.

[10] E. Peled, The electrochemical-behavior of alkali and alkaline-earth metals in nonaqueous battery systems - the solid electrolyte interphase model, J. Electrochem. Soc. 126 (1979) 2047–2051, http://dx.doi.org/10.1149/1.2128859.

[11] H.M. Jung, S.-H. Park, J. Jeon, Y. Choi, S. Yoon, J.-J. Cho, S. Oh, S. Kang, Y.-K. Han, H. Lee, Fluoropropane sultone as an SEI-forming additive that outperforms vinylene carbonate, J. Mater. Chem. A 1 (2013) 11975–11981, http://dx.doi.org/10.1039/c3ta12580g.

[12] N.N. Sinha, J.C. Burns, J.R. Dahn, Storage studies on Li/Graphite cells and the impact of so-called SEI-forming electrolyte additives, J. Electrochem. Soc. 160 (2013) A709–A714, http://dx.doi.org/10.1149/2.008306jes.

[13] S.E. Sloop, J.K. Pugh, S. Wang, J.B. Kerr, K. Kinoshita, Chemical reactivity of PF_5 and $LiPF_6$ in ethylene carbonate/dimethyl carbonate solutions, Electrochem. Solid-State Lett. 4 (2001), http://dx.doi.org/10.1149/1.1353158 A42.

[14] K. Xu, S. Zhang, T.R. Jow, W. Xu, C.A. Angell, LiBOB as salt for lithium-ion batteries:a possible solution for high temperature operation, Electrochem. Solid-State Lett. 5 (2002), http://dx.doi.org/10.1149/1.1426042 A26.

[15] a.M. Andersson, K. Edström, Chemical composition and morphology of the elevated temperature SEI on graphite, J. Electrochem. Soc. 148 (2001), http://dx.doi.org/10.1149/1.1397771 A1100.

[16] K. Araki, N. Sato, Chemical transformation of the electrode surface of lithium-ion battery after storing at high temperature, J. Power Sources 124 (2003) 124–132, http://dx.doi.org/10.1016/S0378-7753(03)00593-7.

[17] L. Bodenes, R. Dedryvere, H. Martinez, F. Fischer, C. Tessier, J.-P. Peres, Lithium-ion batteries working at 85 C: aging phenomena and electrode/electrolyte interfaces studied by XPS, J. Electrochem. Soc. 159 (2012) A1739–A1746, http://dx.doi.org/10.1149/2.061210jes.

[18] S. Grugeon, S. Laruelle, L. Dupont, J.M. Tarascon, An update on the reactivity of nanoparticles co-based compounds towards Li, Solid State Sci. 5 (2003) 895–904, http://dx.doi.org/10.1016/S1293-2558(03)00114-6.

[19] N. Pereira, M. Balasubramanian, L. Dupont, J. McBreen, L.C. Klein, G.G. Amatucci, The electrochemistry of germanium nitride with lithium, J. Electrochem. Soc. 150 (2003), http://dx.doi.org/10.1149/1.1587724 A1118.

[20] F. Mestre-Aizpurua, S. Laruelle, S. Grugeon, J.-M. Tarascon, M.R. Palacín, High temperature lithium cells using conversion oxide electrodes, J. Appl. Electrochem. 40 (2010) 1365–1370, http://dx.doi.org/10.1007/s10800-010-0103-0.

[21] M.F. Hassan, M.M. Rahman, Z.P. Guo, Z.X. Chen, H.K. Liu, Solvent-assisted molten salt process: a new route to synthesis α-Fe_2O_3/C nanocomposite and its electrochemical performance in lithium-ion batteries, Electrochim. Acta 55 (2010) 5006–5013, http://dx.doi.org/10.1016/j.electacta.2010.04.006.

[22] M.F. Hassan, Z. Guo, Z. Chen, H. Liu, α-Fe_2O_3 as an anode material with capacity rise and high rate capability for lithium-ion batteries, Mater. Res. Bull. 46 (2011) 858–864, http://dx.doi.org/10.1016/j.materresbull.2011.02.011.

[23] P. Poizot, S. Laruelle, S. Grugeon, L. Dupont, J.-M. Tarascon, From the vanadates to 3d-metal oxides negative electrodes, Ionics (Kiel) 6 (2000) 321–330, http://dx.doi.org/10.1007/BF02374148.

[24] S. Laruelle, S. Grugeon, P. Poizot, M. Dollé, L. Dupont, J.-M. Tarascon, On the origin of the extra electrochemical capacity displayed by MO/Li cells at low potential, J. Electrochem. Soc. 149 (2002), http://dx.doi.org/10.1149/1.1467947 A627.

[25] L. Gireaud, S. Grugeon, S. Laruelle, S. Pilard, J.-M. Tarascon, Identification of Li battery electrolyte degradation products through direct synthesis and characterization of alkyl carbonate salts, J. Electrochem. Soc. 152 (2005), http://dx.doi.org/10.1149/1.1872673 A850.

[26] S. Laruelle, S. Pilard, P. Guenot, S. Grugeon, J.-M. Tarascon, Identification of Li-Based electrolyte degradation products through DEI and ESI high-resolution mass spectrometry, J. Electrochem. Soc. 151 (2004), http://dx.doi.org/10.1149/1.1760992 A1202.

[27] L. Gireaud, S. Grugeon, S. Pilard, P. Guenot, J.-M. Tarascon, S. Laruelle, Mass spectrometry investigations on electrolyte degradation products for the development of nanocomposite electrodes in lithium ion batteries, Anal. Chem. 78 (2006) 3688–3698, http://dx.doi.org/10.1021/ac051987w.

[28] R. Dedryvère, S. Laruelle, S. Grugeon, P. Poizot, D. Gonbeau, J.M. Tarascon, Contribution of x-ray photoelectron spectroscopy to the study of the electrochemical reactivity of CoO toward lithium, Chem. Mater. 16 (2004) 1056–1061, http://dx.doi.org/10.1021/cm0311269.

[29] J.-M. Tarascon, S. Grugeon, M. Morcrette, S. Laruelle, P. Rozier, P. Poizot, New concepts for the search of better electrode materials for rechargeable lithium batteries, Compt. Rendus Chem. 8 (2005) 9–15, http://dx.doi.org/10.1016/j.crci.2004.12.005.

[30] P. Balaya, H. Li, L. Kienle, J. Maier, Fully reversible homogeneous and heterogeneous Li storage in RuO_2 with high capacity, Adv. Funct. Mater. 13 (2003) 621–625, http://dx.doi.org/10.1002/adfm.200304406.

[31] K.H. Seng, L. Li, D.P. Chen, Z.X. Chen, X.L. Wang, H.K. Liu, Z.P. Guo, The effects of FEC (fluoroethylene carbonate) electrolyte additive on the lithium storage properties of NiO (nickel oxide) nanocuboids, Energy 58 (2013) 707–713, http://dx.doi.org/10.1016/j.energy.2013.06.011.

[32] M.T. Sougrati, J. Fullenwarth, a. Debenedetti, B. Fraisse, J.C. Jumas, L. Monconduit, TiSnSb a new efficient negative electrode for Li-ion batteries: mechanism investigations by operando-XRD and Mössbauer techniques, J. Mater. Chem. 21 (2011) 10069, http://dx.doi.org/10.1039/c1jm10710k.

[33] H.A. Wilhelm, C. Marino, A. Darwiche, P. Soudan, M. Morcrette, L. Monconduit, B. Lestriez, Engineering study on TiSnSb-based composite negative electrode for Li-ion batteries, J. Power Sources 274 (2015) 496–505, http://dx.doi.org/10.1016/j.jpowsour.2014.10.051.

[34] H.A. Wilhelm, C. Marino, A. Darwiche, L. Monconduit, B. Lestriez, Significant electrochemical performance improvement of TiSnSb as anode material for Li-ion batteries with composite electrode formulation and the use of VC and FEC electrolyte additives, Electrochem. Commun. 24 (2012) 89–92, http://dx.doi.org/10.1016/j.elecom.2012.08.023.

[35] E. Dashjav, H. Kleinke, Sn/Sb atom ordering in the ternary stannide-antimonide TiSnSb, J. Solid State Chem. 176 (2003) 329–337, http://dx.doi.org/10.1016/S0022-4596(03)00214-7.

[36] D.A. Shirley, High-resolution x-ray photoemission spectrum of the valence bands of gold, Phys. Rev. B 5 (1972) 4709–4714, http://dx.doi.org/10.1103/PhysRevB.5.4709.

[37] W. Zhang, F. Ghamouss, A. Darwiche, L. Monconduit, D. Lemordant, R. Dedryvère, H. Martinez, Surface film formation on TiSnSb electrodes: impact of electrolyte additives, J. Power Sources 268 (2014) 645–657, http://dx.doi.org/10.1016/j.jpowsour.2014.06.041.

[38] S. Wilken, M. Treskow, J. Scheers, P. Johansson, P. Jacobsson, Initial stages of thermal decomposition of LiPF6-based lithium ion battery electrolytes by detailed Raman and NMR spectroscopy, RSC Adv. 3 (2013) 16359–16364, http://dx.doi.org/10.1039/c3ra42611d.

[39] D. Pantea, H. Darmstadt, S. Kaliaguine, L. Sümmchen, C. Roy, Electrical conductivity of thermal carbon blacks, Carbon N. Y. 39 (2001) 1147–1158, http://dx.doi.org/10.1016/S0008-6223(00)00239-6.

[40] D. Pantea, H. Darmstadt, S. Kaliaguine, C. Roy, Electrical conductivity of conductive carbon blacks: influence of surface chemistry and topology, Appl. Surf. Sci. 217 (2003) 181–193, http://dx.doi.org/10.1016/S0169-4332(03)00550-6.

[41] L. El Ouatani, R. Dedryvère, C. Siret, P. Biensan, S. Reynaud, P. Iratçabal, D. Gonbeau, The effect of vinylene carbonate additive on surface film formation on both electrodes in Li-Ion batteries, J. Electrochem. Soc. 156 (2009), http://dx.doi.org/10.1149/1.3029674 A103.

[42] L. Madec, J. Xia, R. Petibon, K.J. Nelson, J.-P. Sun, I.G. Hill, J.R. Dahn, Effect of sulfate electrolyte additives on $LiNi_{1/3}Mn_{1/3}Co_{1/3}O_2$/graphite pouch cell lifetime: correlation between XPS surface studies and electrochemical test results, J. Phys. Chem. C 118 (2014) 29608–29622, http://dx.doi.org/10.1021/jp509731y.

[43] A. Darwiche, L. Bodenes, L. Madec, L. Monconduit, H. Martinez, Impact of the salts and solvents on the SEI formation in Sb/Na batteries: an XPS analysis, Electrochim. Acta 207 (2016) 284–292, http://dx.doi.org/10.1016/j.electacta.2016.03.089.

[44] K. Ciosek Högström, S. Malmgren, M. Hahlin, M. Gorgoi, L. Nyholm, H. Rensmo, K. Edström, The buried carbon/solid electrolyte interphase in Li-ion batteries studied by hard x-ray photoelectron spectroscopy, Electrochim. Acta 138 (2014) 430–436, http://dx.doi.org/10.1016/j.electacta.2014.06.129.

[45] D. Aurbach, Identification of surface films formed on lithium in propylene carbonate solutions, J. Electrochem. Soc. 134 (1987) 1611–1620, http://dx.doi.org/10.1149/1.2100722.

[46] M. Nie, D.P. Abraham, Y. Chen, A. Bose, B.L. Lucht, Silicon solid electrolyte interphase (SEI) of lithium ion battery characterized by microscopy and spectroscopy silicon solid electrolyte interphase (SEI) of lithium ion battery characterized by microscopy and spectroscopy, J. Phys. Chem. C 117 (2013) 1257–1267, http://dx.doi.org/10.1021/jp404155y.

[47] R. Dedryvère, L. Gireaud, S. Grugeon, S. Laruelle, J.M. Tarascon, D. Gonbeau, Characterization of lithium alkyl carbonates by X-ray photoelectron spectroscopy: experimental and theoretical study, J. Phys. Chem. B 109 (2005) 15868–15875, http://dx.doi.org/10.1021/jp051626k.

[48] S. Malmgren, K. Ciosek, M. Hahlin, T. Gustafsson, M. Gorgoi, H. Rensmo, K. Edström, Comparing anode and cathode electrode/electrolyte interface composition and morphology using soft and hard X-ray photoelectron spectroscopy, Electrochim. Acta 97 (2013) 23–32, http://dx.doi.org/10.1016/j.electacta.2013.03.010.

[49] L. El Ouatani, R. Dedryvère, C. Siret, P. Biensan, D. Gonbeau, Effect of vinylene carbonate additive in Li-ion batteries: comparison of $LiCoO_2$/C, $LiFePO_4$/C, and $LiCoO_2$/$Li_4Ti_5O_{12}$ systems, J. Electrochem. Soc. 156 (2009), http://dx.doi.org/10.1149/1.3111891 A468.